Theoretical study of (*e*, 2*e*) processes for valence orbitals of CH₄ using a multicenter distorted-wave method

Maomao Gong,[1,*] Xingyu Li,[1,2] Song Bin Zhang,[3] Ling Liu,[2] Yong Wu,[2] Jianguo Wang,[2] Yizhi Qu,[4] and Xiangjun Chen[1,†]

[1]*Hefei National Laboratory for Physical Sciences at Microscale and Department of Modern Physics,*
University of Science and Technology of China, Hefei, Anhui 230026, China
[2]*Data Center for High Energy Density Physics, Institute of Applied Physics and Computational Mathematics, Beijing 100088, China*
[3]*School of Physics and Information Technology, Shaanxi Normal University, Xi'an 710119, China*
[4]*College of Material Sciences and Optoelectronic Technology, University of the Chinese Academy of Sciences, Beijing 100049, China*

A multicenter distorted-wave method is used to study the electron impact single ionization from the outer $(1t_2)$ and inner $(2a_1)$ valence orbitals of a CH₄ molecule. The triple differential cross sections are calculated in coplanar asymmetric kinematics with the scattered electron energy at 500 eV and the ejected electron energy at 12, 37, and 74 eV, respectively. The nuclear term in the ionization transition amplitude is fully included, and the calculated results well reproduce the experimental measurements, especially for the $2a_1$ orbital, where excellent agreement has been achieved.

I. INTRODUCTION

The triple differential cross section (TDCS) for $(e,2e)$ process is a measure of the probability of detecting ejected electron with a specific energy emerges at given angles for selected initial and final momenta of the projectile. During the last decades, many measurements have been carried out for different molecular targets, including H₂ [1–3], N₂ [4–6], H₂O [7], CO₂ [4,8], N₂O [9], CH₄ [10], and HCOOH [11], as well as the more complex ones such as phenol [12], furfural [13], and para-benzoquinone [14]. It still remains a big challenge to explain the experimental results accurately, especially for the ionization of molecule due to its multicenter nature as well as the complex electronic structure. Most of the $(e,2e)$ experiments are not able to study oriented molecules and molecules with arbitrary orientations contribute to the experiments equally; therefore in the theoretical calculations one must average over all the possible molecular orientations before comparing with the experimental data. This makes the calculations even more costly.

Various kinds of theoretical methods have been developed to treat this problem, including nonperturbative [15–17] and perturbative [18–33] approaches. The nonperturbative approaches, such as the time-dependent close-coupling method [15], the converged close-coupling method [16], as well as the exterior complex scaling method [17], are usually limited to simple diatomic molecules [3,34–39] and the extension to more complex polyatomic molecules encounters practical difficulties.

For the perturbative approaches, the distorted-wave impulse approximation [18] and the distorted-wave Born approximation [19] are the two commonly used methods. Madison and coworkers [20–26] developed a molecular three-body distorted-wave (M3DW) model in which the incident, scattered, and ejected continuum wave functions are solved under the spherically averaged potentials, and the orientation-averaged molecular orbital (OAMO) approximation has been introduced to make the practical calculations possible. In the OAMO approximation, instead of averaging over orientation-dependent cross sections, the orientation-dependent molecular orbitals are averaged to obtain a spherically symmetric molecular orbital to be used in the cross-sectional calculations. Recently, a proper average of cross sections over all molecular orientations has been adopted by the same authors when calculating the TDCSs of CH₄ [27] and C₂H₆ [28] using the M3DW method. Another kind of perturbative method is the Brauner, Briggs, and Klar (BBK) model, also known as the three-Coulomb wave model [29,30]. Because of its shortcoming in describing the distorted wave function, BBKDW [31,32] and BBKSR [32] models were developed quite recently to include the distorted wave effects. BBKDW used the spherically symmetric potential to represent Coulomb potential, while BBKSR included the short range potential in the pure Coulomb model. But these sophisticated perturbative models still have obvious weaknesses in describing the final continuum wave function. The multicenter nature of molecule which is important in the calculation was ignored.

Very recently, the multicenter nature of molecule is taken into consideration in both the complex Kohn treatment [40,41] and our MCDW method [42,43] in the calculation of the final ejected wave function. The TDCS is then averaged over all possible orientations. It is worth mentioning that both two methods make the assumption that the incident and scattered electron are fast enough to be described as the plane waves. This assumption could reduce the computational efforts significantly, but limits the studies to the asymmetric kinematics. Complex Kohn treatment is based on complex Kohn variational method, and the interaction between the slow ejected electron and the residual molecular ion is treated by a close coupling method precisely. Good agreement has been achieved with the experiments in the applications to H₂O [40] and CH₄ [41]. In the MCDW method, the continuum wave function of the slow ejected electron is calculated in the potential of the residual ion under the sudden approximation. Through this way the influence of the anisotropic multicenter nature on the slow ejected electron has been taken

_____

*gongmm@mail.ustc.edu.cn
†xjun@ustc.edu.cn

into account largely. The MCDW method was applied to calculate the TDCSs of H_2O [42], and recently been extended to the MCDW-NT (MCDW-NuclearTerm) model to fully include the nuclear term in the case of HCOOH [43]. The calculated results for both molecules show good agreement with the experiments.

In the present work, we use the MCDW-NT model to calculate the TDCSs of the outer ($1t_2$) and inner ($2a_1$) valence orbitals of CH_4. The experimental measurements were carried out by Lahham-Bennani *et al.* [10] in coplanar asymmetric kinematics with the scattered electron energy at 500 eV, ejected electron energy at 12, 37, and 74 eV, and scattering angle of the fast outgoing electron at $-6°$. The experimental results were compared with theoretical ones using the simple 1CW model (where only the ejected electron is described by a Coulomb wave) and the BBK model [10]. The experimental cross sections exhibited a very strong recoil scattering, especially for the inner $2a_1$ molecular orbital, which was not predicted by the theory. The authors attributed the failure of theory to improper description of the strong scattering from the ion. In the present MCDW-NT calculations, the continuum wave function of ejected electron is solved in the potential of residual ion, and the nuclear term in the ionization transition amplitude is fully included. The results show that the large recoil peaks are reasonably reproduced. The paper is organized as follows: in the next section we briefly outline the MCDW method. The results and comparisons with experimental data and other calculations as well as discussions will be presented in Sec. 3, followed by the summary in Sec. 4. Atomic units are used throughout the paper unless explicitly stated otherwise.

II. THEORETICAL METHOD

The details of the MCDW method have been given in Refs. [42,43]; here we only briefly outline its formulation. In general scattering theory, the initial state of the $N + 1$-electron system is the product of a bound molecular state and a plane wave which describes the incident electron. If the whole interaction between the incident electron and the molecular target is taken as the scattering potential, the final state can be written as a product of the wave functions describing molecular ion, ejected electron, and scattered electron in the frame of the first Born approximation (FBA). The transition amplitude for a given molecular orientation in a laboratory frame reads

$$T_{fi}(\Omega) = \langle \boldsymbol{k}_s \Psi_f^{(-)}(\boldsymbol{k}_e; \mathcal{R}_\Omega^{-1}\{\boldsymbol{r}\}) | V(\{\boldsymbol{r}\}) | \boldsymbol{k}_i \Psi_i(\mathcal{R}_\Omega^{-1}\{\boldsymbol{r}\}) \rangle, \quad (1)$$

where $\boldsymbol{k}_i$, $\boldsymbol{k}_s$, and $\boldsymbol{k}_e$ represent the momenta of the incident, scattered, and ejected electrons, respectively. The molecular orientation is defined by Euler angle $\Omega = (\alpha, \beta, \gamma)$. Operator $\mathcal{R}_\Omega^{-1}$ represents the rotation of the target. $|\Psi_i\rangle$ is the initial bound wave function, and $\{\boldsymbol{r}\}$ refers to the set of electronic coordinates. In final state $|\Psi_f\rangle$, the ionized orbital is substituted by the continuum wave function of the ejected electron. The incident and scattered electrons are described by the plane waves $|\boldsymbol{k}_i\rangle$ and $|\boldsymbol{k}_s\rangle$. With the help of the Bethe integral, the system can be simplified as a one-active-electron problem under the sudden approximation, giving rise to the following

expression:

$$T_{fi}(\Omega) = \frac{4\pi}{K^2}\langle \mathcal{F}^{(-)}(\boldsymbol{k}_e; \mathcal{R}^{-1}\boldsymbol{r}_e)|e^{i\boldsymbol{K}\cdot\boldsymbol{r}_e} - \frac{\sum_n Z_n e^{i\boldsymbol{K}\cdot\boldsymbol{R}_n}}{N}$$
$$\times |\phi_\alpha(\mathcal{R}^{-1}\boldsymbol{r}_e)\rangle, \quad (2)$$

where $\boldsymbol{K} = \boldsymbol{k}_i - \boldsymbol{k}_s$ is the momentum transfer. $\boldsymbol{R}_n$ is the position of the nth nucleus, and Z_n indicates its charge. Vector $\boldsymbol{r}_e$ represents the position of the active electron. $|\mathcal{F}^{(-)}\rangle$ is the continuum wave function of the ejected electron, and $|\phi_\alpha\rangle$ is the bound orbital to be ionized. The first term in Eq. (2) represents the scattering by the active electron, and the second term refers to the scattering by the nuclei. This nuclear term will be vanished if the initial bound state is orthogonal to the final continuum state. However, in the present model, the continuum wave function of the ejected electron is solved under the single-active-electron approximation and is generally not orthogonal to the bound orbital $|\phi_\alpha\rangle$. Therefore, this term will be fully included in the present calculation, and the method is termed MCDW-NT.

The TDCS is then obtained by averaging over all possible molecular orientations:

$$\frac{d^5\sigma}{d\Omega_e d\Omega_s dE_s} = G\frac{1}{(2\pi)^5}\frac{k_e k_s}{k_i}\frac{1}{8\pi^2}\int |T_{fi}(\Omega)|^2 d\Omega, \quad (3)$$

where G is the electron occupation number of the ionized molecular orbital.

To solve the continuum wave function, the ejected electron is regarded as moving in the anisotropic field of the residual ion, while the interaction from the fast scattering electron is neglected. A model potential is adopted [42]:

$$V^m = V^{st} + V^{cp} + V^{model\ exc}, \quad (4)$$

where V^{st} is the electrostatic potential between the incident electron and residual molecular ion. V^{cp} and $V^{model\ exc}$ are the correlation-polarization potential and the model exchange potential, respectively.

The effective Schrödinger equation for the ejected electron is

$$\left[-\tfrac{1}{2}\nabla^2 + V^m - E_{k_e}\right]\mathcal{F}^{(-)}(\boldsymbol{k}_e; \boldsymbol{r}_e) = 0. \quad (5)$$

The anisotropic multicenter feature of $\mathcal{F}^{(-)}(\boldsymbol{k}_e; \boldsymbol{r}_e)$ is inherited from V^m. To solve this equation, the single-centered expansion technique [44–46] is employed, where the wave function and potential are expanded over the symmetry-adapted angular functions. Note that the model potential V^m is anisotropic and introduces couplings between terms of different angular momentum in the partial wave expansion of $\mathcal{F}^{(-)}(\boldsymbol{k}_e; \boldsymbol{r}_e)$, resulting in a set of coupled equations. As shown in our previous work [42,43], the diagonal terms in the potential matrix are considered dominant. Thus in practical calculation, we will ignore the off-diagonal elements and solve the decoupled partial wave equations.

III. RESULTS AND DISCUSSION

The methane molecule (CH_4) belongs to the T_d symmetry point group, and its ground state is nominally described by the configuration $1a_1^2 2a_1^2 1t_2^6$. In the present work, the TDCSs for the electron impact ionizations from the outer
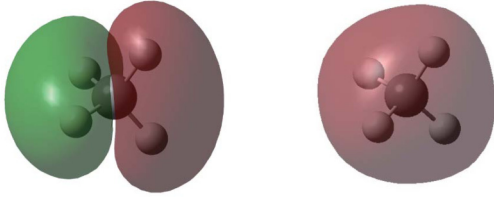
FIG. 1. Illustrations of molecular orbitals $1t_2$ (left) and $2a_1$ (right).

($1t_2$) and inner ($2a_1$) valence molecular orbitals (MOs) of CH_4 have been calculated using MCDW-NT method. The experiments were carried out by Lahham-Bennani *et al.* [10] in the coplanar asymmetric kinematics with $E_e = 12, 37$, and 74 eV, $E_s = 500$ eV, and $\theta_s = -6°$. The incident electron energy is consequently given by the energy conservation, $E_i = E_e + E_s +$ IP, where IP is the ionization potential of the corresponding MO. According to Lahham-Bennani *et al.*, the IPs of $1t_2$ and $2a_1$ orbitals are 14.25 and 25.73 eV, respectively. In our calculations, more accurate experimental values of 12.51 and 22.4 eV [47] are used instead. All our calculations are performed at equilibrium geometry with a C-H bond length of 1.087 Å [48]. The wave functions of the MOs of CH_4 are calculated using the Gaussian 09 [49] program with the density functional theory method employing B3LYP hybrid functional [50,51] and the cc-pVTZ basis set [52]. The calculated MOs are then expanded into the symmetry-adapted angular functions. Let $l_{b\max}$ and $l_{c\max}$ denote the upper limits of the angular momentum in the partial wave expansions for the bound orbital and continuum wave functions, respectively, and the convergence is reached with $l_{b\max} = 10$ and $l_{c\max} = 25$ in our calculations. In the single-center expansion, r ranges from 0 to 8.47 a.u. with increasing step size from 0.01 to 0.128 a.u.. The convergence of the numerical spherical average is achieved with the Euler angle mesh $N_\alpha = N_\beta = N_\gamma = 18$, where N_α, N_β, and N_γ represent the number of points for Euler angle α, β, and γ, respectively. The orbital maps of the two MOs are illustrated in Fig. 1, showing that $1t_2$ is of sp-type and $2a_1$ is of s-type.

The TDCSs for orbitals $1t_2$ and $2a_1$ are shown in Figs. 2 and 3 in which the ejection angle is defined as the angle of ejected electron with respect to the incident direction. The relative experimental data are normalized to our MCDW-NT calculations at the binary peak. The experimental results for the two orbitals both show a typical two-lobe structure. The binary peak is located around momentum transfer direction($\boldsymbol{K}$). In the sudden approximation, the binary peak could be considered as the result of the binary collision between incident and target electron. While the recoil peak around the opposite direction of momentum transfer($-\boldsymbol{K}$) is usually smaller in magnitude and broader than the binary peak, which is generally explained as quantal backward reflection in the potential well of the residual ion. For comparison, we also plot theoretical results calculated by the complex Kohn variational method [41] as well as the BBK model [10] after proper scaling. In the case of $E_e = 74$ eV, the BBKSR result [32] is also included.

Figures 2(a)–2(c) show the results for orbital $1t_2$ at $E_e = 12, 37$, and 74 eV, respectively. For the binary peak at $E_e = 12$ eV, the experimental data exhibits a very weak splitting as shown in Fig. 2(a). This can be attributed to the carbon $2p$
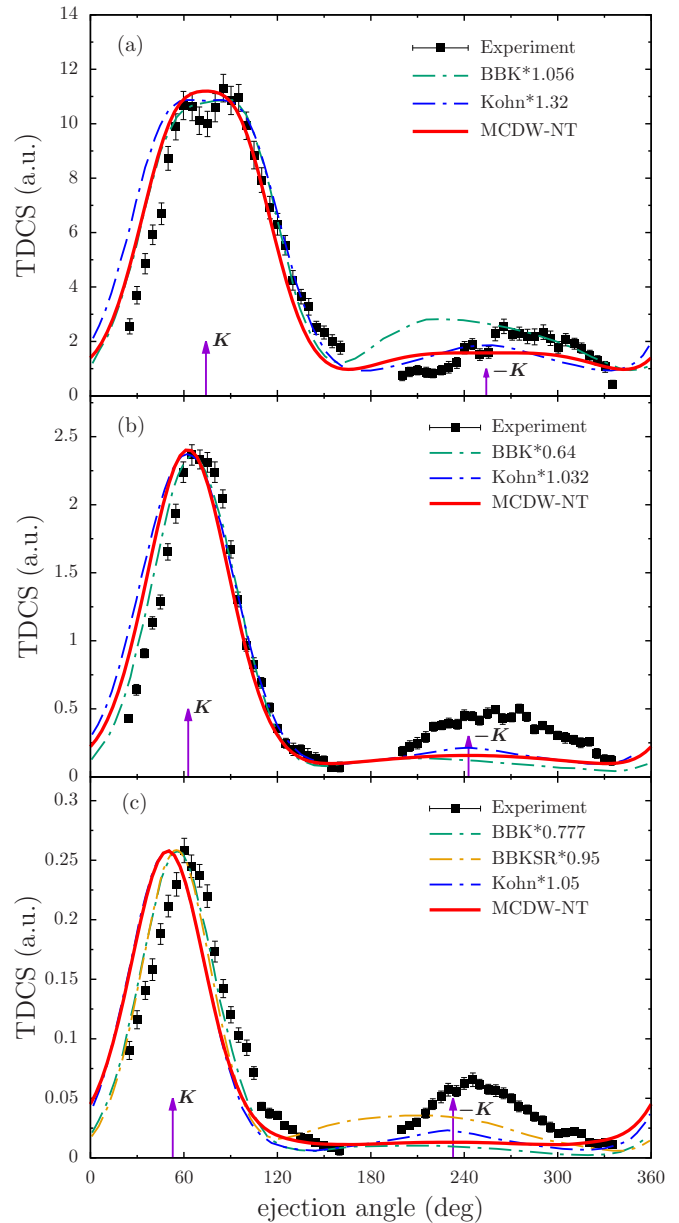

FIG. 2. TDCSs for electron impact ionization of the out-valence ($1t_2$) orbital of methane in coplanar geometry. The experimental measurements (squared points)) were carried out by A Lahham-Bennani *et al.* [10] in the coplanar asymmetric kinematics. The scattered electron energy and the scattering angle are 500 eV and $-6°$, respectively. The ejected electron energy and its corresponding magnitude of the momentum transfers are (a) $E_e = 12$ eV, $|\boldsymbol{K}| = 0.659$ a.u., (b) $E_e = 37$ eV, $|\boldsymbol{K}| = 0.713$ a.u., and (c) $E_e = 74$ eV, $|\boldsymbol{K}| = 0.83$ a.u., respectively. All the experimental data and theoretical results have been normalized to the binary peak maximum of MCDW-NT theory (red solid line). The complex Kohn results (blue dashed line) have been multiplied by (a) 1.32, (b) 1.032, and (c) 1.05, respectively. While the BBK (BBKSR) results are multiplied by (a) 1.056, (b) 0.64, and (c) 0.777 (0.95).

character of the $1t_2$ orbital. This weak splitting disappears with the increasing of the ejected electron energy. The shapes of the binary peak for all three ejected energies are well described by our MCDW-NT calculations. The complex Kohn and BBK
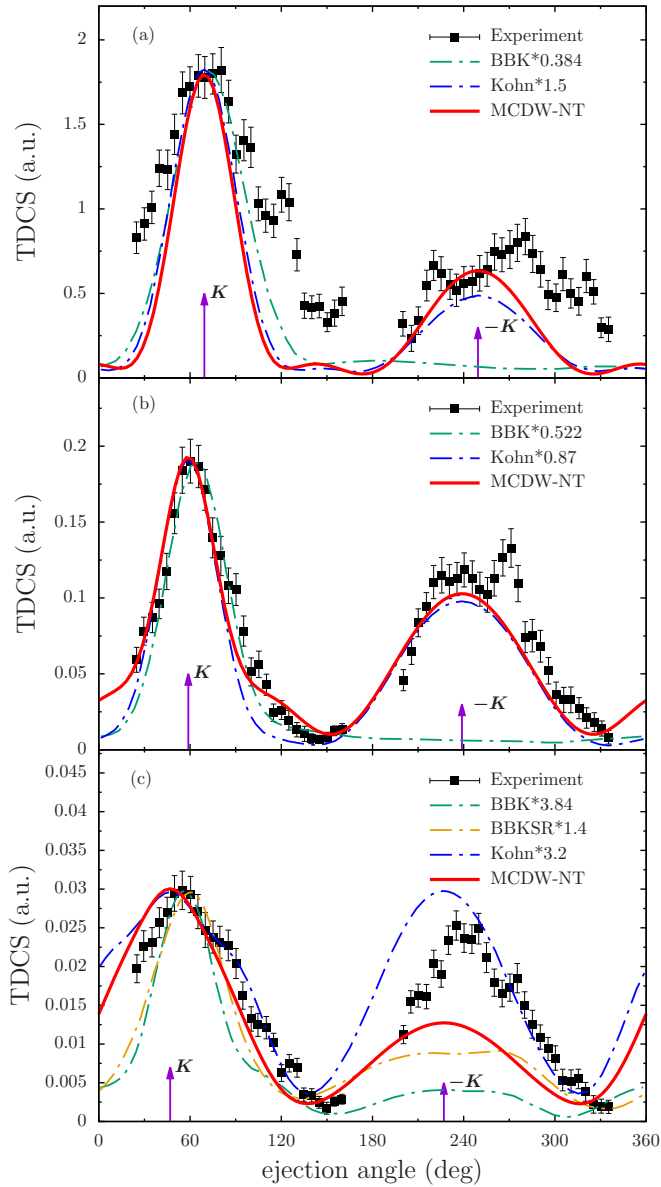
FIG. 3. Same as in Fig. 2 but for inner-valence ($2a_1$) orbital. The ejected electron energy and its corresponding magnitude of the momentum transfers are (a) $E_e = 12$ eV, $|\mathbf{K}| = 0.677$ a.u., (b) $E_e = 37$ eV, $|\mathbf{K}| = 0.74$ a.u., and (c) $E_e = 74$ eV, $|\mathbf{K}| = 0.867$ a.u., respectively. The complex Kohn results have been multiplied by (a) 1.5, (b) 0.87, (c) 3.2, respectively. While the BBK (BBKSR) results are multiplied by (a) 0.384, (b) 0.552, (c) 3.84 (1.4).

methods also reproduce the shapes of the binary peak quite well. The complex Kohn method predicts a little bit wider binary peak at $E_e = 12$ eV but clearly shows a weak splitting. At $E_e = 74$ eV, the experimental binary peak is shifted approximately by $10°$ towards larger ejection angles than our MCDW-NT method and the complex Kohn treatment. This shift can be partially attributed to the postcollision interaction (PCI), which is not included in the present calculations. In the case of a slow ejected electron, the scattering electron leaves the target much faster than the ejected electron, and the interaction between the ejected and scattering electron is weak. As the ejected energy increases, this interaction becomes

more pronounced. As can be seen in the figures, the BBK and BBKSR models predict more accurate binary peak positions, owing to the use of 3-Coulomb (3C) wave functions which naturally consider the PCI effect.

All the theoretical models fail to reproduce both the structure and the magnitude of the recoil peak for orbital $1t_2$. With the increasing of the ejected electron energy, the ratio between the binary and recoil peaks of the experimental data does not change too much and approximately equals 4.0–5.0. However, all the calculations predict a sharp change. The magnitude of the recoil peak can be moderately described at $E_e = 12$ eV by the complex Kohn and our MCDW-NT methods, but are underestimated at $E_e = 37$ and 74 eV, while the BBK model predicts a stronger recoil peak at $E_e = 12$ eV but much weaker ones at $E_e = 37$ and 74 eV. The BBKSR calculation, which is available only at $E_e = 74$ eV, predicts a higher recoil peak at this energy. The positions of the recoil peaks of the BBK (BBKSR) results are even smaller than the results of the complex Kohn and our MCDW-NT methods, largely deviated from the measurements.

The TDCSs for orbital $2a_1$ are shown in Figs. 3(a)–3(c) with $E_e = 12$, 37, and 74 eV, respectively. Differently from the results of $1t_2$ orbital, the experimental data shows a pronounced recoil peak in each case. In Fig. 3(a), our MCDW-NT model predicts a much narrower binary peak than the experimental data but well describes the peak position. The complex Kohn treatment and BBK model also present the similar results. For the recoil peak in Fig. 3(a), our MCDW-NT method shows better agreement with the experiment than the complex Kohn treatment. The BBK model fails to reproduce the recoil peak. For $E_e = 37$ eV in Fig. 3(b), excellent agreement between the measurement and our MCDW-NT calculation has been achieved in both the binary and recoil regions. Complex Kohn treatment presents the similar results with the present calculations, while the BBK model still cannot reproduce the recoil peak. As for $E_e = 74$ eV in Fig. 3(c), our MCDW-NT calculation displays broad binary and large recoil peaks. The agreement between present model and experiment is moderate. But big discrepancies from the experiment still exist, especially in the recoil region. It is worth noting that MCDW-NT method gives a lower recoil peak than the experimental data in Fig. 3(c), while complex Kohn treatment produces an opposite outcome. This partly reflects the difference between the calculation models. The final continuum wave function of the ejected electron is calculated in the multicenter potential of the residual ion in our MCDW-NT method. And in the complex Kohn treatment, the final wave function is solved by close coupling method. As for the BBK model, it fails to interpret the experiment in both binary and recoil regions except the correct binary peak position. The results of the BBKSR model [32] predict a larger recoil peak, indicating that the short range potential can be important in the calculation. It is not surprising because the short-range potential could have great effect on the dynamic process of the ejected electron.

With regard to the failure of the BBK model in describing the large recoil intensity observed in the experiment, Lahmam-Bennani *et al.* [10] argued that the quasiabsence of a recoil peak in the BBK perturbative models can be traced to their failure to properly describe the interaction of the ejected

electron with the target nuclei at the kinematic conditions of the CH_4 experiments which are far from the so-called Bethe ridge, where the magnitude of $\boldsymbol{K}$ is close to the momentum of $\boldsymbol{k}_e$. Lin *et al*. [41] further pointed out that kinematic condition is just one of the factors that determine the accuracy of the TDCS in the recoil region. They explained that the employment of an atomic Coulomb function with $Z = -1$ in BBK model is also the reason of failure to reproduce the recoil peak for $2a_1$ ionization, since the strong electron-nuclear interaction is not properly taken into account. In our MCDW-NT calculations, the interaction between the slow ejected electron and the distorted potential of residual ion is largely included, so the large recoil peak for TDCS of $2a_1$ orbital can be easily understood. Therefore we can conclude that the multicenter nature of molecular targets has a significant effect on the final continuum wave function and then affects the accuracy of the calculations of the TDCSs.

IV. SUMMARY

In this paper, the multicenter distorted-wave method has been used to study the (e,2e) TDCSs for the outer ($1t_2$) and inner ($2a_1$) valence orbitals of CH_4 in coplanar asymmetric kinematics with $E_s = 500$ eV, $E_e = 12$, 37, and 74 eV. In the present calculation, the continuum wave function of the ejected electron is solved in the multicenter potential of the residual ion, and the nuclear term in the ionization transition amplitude is fully included. The results are compared with the experimental measurements of Lahmam-Bennani *et al*. [10]. Our MCDW-NT calculations generally reproduce the binary peaks in all cases. For the ionization from the inner-valence $2a_1$ orbital, our calculations are found to present excellent description of the TDCSs in the recoil region where pronounced recoil peaks were observed for all three ejected electron energies by the experiments. However, for the outer-valence $1t_2$ orbital, the recoil peak is only reasonably reproduced at $E_e = 12$ eV, but underestimated at higher energies $E_e = 37$ and 74 eV. As we have mentioned, in practical calculation, we ignore the off-diagonal terms in the potential matrix when solving the continuum wave function of the ejected electron. This may be the reason that the present MCDW-NT model cannot reproduce the recoil peaks for $1t_2$ ionization. Furthermore, the higher-order effects beyond the FBA may also contribute to the discrepancies between present calculations and experiments.

[1] M. Cherid, A. Lahmam-Bennani, A. Duguet, R. W. Zurales, R. R. Lucchese, M. C. D. Cappello, and C. D. Cappello, J. Phys. B **22**, 3483 (1989).

[2] E. M. S. Casagrande, A. Naja, F. Mezdari, A. Lahmam-Bennani, P. Bolognesi, B. Joulakian, O. Chuluunbaatar, O. Al-Hagan, D. H. Madison, D. V. Fursa, and I. Bray, J. Phys. B **41**, 025204 (2008).

[3] J. Colgan, O. Al-Hagan, D. H. Madison, C. Kaiser, A. J. Murray, and M. S. Pindzola, Phys. Rev. A **79**, 052704 (2009).

[4] A. Lahmam-Bennani, E. M. S. Casagrande, and A. Naja, J. Phys. B **42**, 235205 (2009).

[5] L. R. Hargreaves, C. Colyer, M. A. Stevenson, B. Lohmann, O. Al-Hagan, D. H. Madison, and C. G. Ning, Phys. Rev. A **80**, 062704 (2009).

[6] H. Chaluvadi, Z. N. Ozer, M. Dogan, C. Ning, J. Colgan, and D. Madison, J. Phys. B **48**, 155203 (2015).

[7] D. S. Milne-Brownlie, S. J. Cavanagh, B. Lohmann, C. Champion, P. A. Hervieux, and J. Hanssen, Phys. Rev. A **69**, 032701 (2004).

[8] M. J. Hussey and A. J. Murray, J. Phys. B **38**, 2965 (2005).

[9] S. J. Cavanagh and B. Lohmann, J. Phys. B **32**, L261 (1999).

[10] A. Lahmam-Bennani, A. Naja, E. M. S. Casagrande, N. Okumus, C. D. Cappello, I. Charpentier, and S. Houamer, J. Phys. B **42**, 165201 (2009).

[11] C. J. Colyer, M. A. Stevenson, O. Al-Hagan, D. H. Madison, C. G. Ning, and B. Lohmann, J. Phys. B **42**, 235207 (2009).

[12] G. B. da Silva, R. F. C. Neves, L. Chiari, D. B. Jones, E. Ali, D. H. Madison, C. G. Ning, K. L. Nixon, M. C. A. Lopes, and M. J. Brunger, J. Chem. Phys. **141**, 124307 (2014).

[13] D. B. Jones, E. Ali, K. L. Nixon, P. Limão-Vieira, M.-J. Hubin-Franskin, J. Delwiche, C. G. Ning, J. Colgan, A. J. Murray, D. H. Madison, and M. J. Brunger, J. Chem. Phys. **143**, 184310 (2015).

[14] D. B. Jones, E. Ali, C. G. Ning, J. Colgan, O. Ingólfsson, D. H. Madison, and M. J. Brunger, J. Chem. Phys. **145**, 164306 (2016).

[15] M. S. Pindzola, F. Robicheaux, S. D. Loch, J. C. Berengut, T. Topcu, J. Colgan, M. Foster, D. C. Griffin, C. P. Ballance, D. R. Schultz, T. Minami, N. R. Badnell, M. C. Witthoeft, D. R. Plante, D. M. Mitnik, J. A. Ludlow, and U. Kleiman, J. Phys. B **40**, R39 (2007).

[16] I. Bray and A. T. Stelbovics, Phys. Rev. A **46**, 6995 (1992).

[17] C. W. McCurdy and T. N. Rescigno, Phys. Rev. A **56**, R4369(R) (1997).

[18] I. McCarthy and E. Weigold, Phys. Rep. **27**, 275 (1976).

[19] D. H. Madison, R. V. Calhoun, and W. N. Shelton, Phys. Rev. A **16**, 552 (1977).

[20] D. H. Madison and O. Al-Hagan, J. At. Mol. Opt. Phys. **2010**, 1 (2010).

[21] J. Gao, D. H. Madison, and J. L. Peacher, Phys. Rev. A **72**, 032721 (2005).

[22] J. Gao, J. L. Peacher, and D. H. Madison, J. Chem. Phys. **123**, 204302 (2005).

[23] J. Gao, D. H. Madison, and J. L. Peacher, J. Chem. Phys. **123**, 204314 (2005).

[24] J. Gao, D. H. Madison, and J. L. Peacher, Phys. Rev. A **72**, 020701 (2005).

[25] J. Gao, D. H. Madison, J. L. Peacher, A. J. Murray, and M. J. Hussey, J. Chem. Phys. **124**, 194306 (2006).

[26] J. Gao, D. H. Madison, and J. L. Peacher, J. Phys. B **39**, 1275 (2006).

[27] H. Chaluvadi, C. G. Ning, and D. Madison, Phys. Rev. A **89**, 062712 (2014).

[28] E. Ali, X. Ren, A. Dorn, C. Ning, and D. Madison, J. Phys. B **48**, 115201 (2015).

[29] C. R. Garibotti and J. E. Miraglia, Phys. Rev. A **21**, 572 (1980).

[30] M. Brauner, J. S. Briggs, and H. Klar, J. Phys. B **22**, 2265 (1989).

[31] M. Chinoune, S. Houamer, C. D. Cappello, and A. Galstyan, J. Phys. B **49**, 205201 (2016).

[32] S. Houamer, M. Chinoune, and C. D. Cappello, Eur. Phys. J. D **71**, 17 (2017).

[33] C. M. Granados-Castro and L. U. Ancarani, Eur. Phys. J. D **71**, 65 (2017).

[34] J. Colgan, M. S. Pindzola, F. Robicheaux, C. Kaiser, A. J. Murray, and D. H. Madison, Phys. Rev. Lett. **101**, 233201 (2008).

[35] M. S. Pindzola, F. Robicheaux, and J. Colgan, J. Phys. B **38**, L285 (2005).

[36] M. S. Pindzola, F. Robicheaux, S. D. Loch, and J. P. Colgan, Phys. Rev. A **73**, 052706 (2006).

[37] M. S. Pindzola, S. A. Abdel-Naby, J. A. Ludlow, F. Robicheaux, and J. Colgan, Phys. Rev. A **85**, 012704 (2012).

[38] M. C. Zammit, D. V. Fursa, and I. Bray, Phys. Rev. A **87**, 020701 (2013).

[39] V. V. Serov and B. B. Joulakian, Phys. Rev. A **80**, 062713 (2009).

[40] C.-Y. Lin, C. W. McCurdy, and T. N. Rescigno, Phys. Rev. A **89**, 012703 (2014).

[41] C.-Y. Lin, C. W. McCurdy, and T. N. Rescigno, Phys. Rev. A **89**, 052718 (2014).

[42] S. B. Zhang, X. Y. Li, J. G. Wang, Y. Z. Qu, and X. Chen, Phys. Rev. A **89**, 052711 (2014).

[43] X. Li, M. Gong, L. Liu, Y. Wu, J. Wang, Y. Qu, and X. Chen, Phys. Rev. A **95**, 012703 (2017).

[44] N. Sanna and F. Gianturco, Comput. Phys. Commun. **128**, 139 (2000).

[45] N. Sanna and G. Morelli, Comput. Phys. Commun. **162**, 51 (2004).

[46] N. Sanna, I. Baccarelli, and G. Morelli, Comput. Phys. Commun. **180**, 2544 (2009).

[47] J. A. R. Samson, G. N. Haddad, T. Masuoka, P. N. Pareek, and D. A. L. Kilcoyne, J. Chem. Phys. **90**, 6925 (1989).

[48] E. Hirota, J. Mol. Spectrosc. **77**, 213 (1979).

[49] M. J. Frisch, G. W. Trucks, H. B. Schlegel, G. E. Scuseria, M. A. Robb, J. R. Cheeseman, G. Scalmani, V. Barone, G. A. Petersson, H. Nakatsuji, X. Li, M. Caricato, A. Marenich, J. Bloino, B. G. Janesko, R. Gomperts, B. Mennucci, H. P. Hratchian, J. V. Ortiz, A. F. Izmaylov, J. L. Sonnenberg, D. Williams-Young, F. Ding, F. Lipparini, F. Egidi, J. Goings, B. Peng, A. Petrone, T. Henderson, D. Ranasinghe, V. G. Zakrzewski, J. Gao, N. Rega, G. Zheng, W. Liang, M. Hada, M. Ehara, K. Toyota, R. Fukuda, J. Hasegawa, M. Ishida, T. Nakajima, Y. Honda, O. Kitao, H. Nakai, T. Vreven, K. Throssell, J. A. Montgomery, Jr., J. E. Peralta, F. Ogliaro, M. Bearpark, J. J. Heyd, E. Brothers, K. N. Kudin, V. N. Staroverov, T. Keith, R. Kobayashi, J. Normand, K. Raghavachari, A. Rendell, J. C. Burant, S. S. Iyengar, J. Tomasi, M. Cossi, J. M. Millam, M. Klene, C. Adamo, R. Cammi, J. W. Ochterski, R. L. Martin, K. Morokuma, O. Farkas, J. B. Foresma, and D. J. Fox, Gaussian 09, Revision A.02, Technical Report.

[50] A. D. Becke, J. Chem. Phys. **98**, 5648 (1993).

[51] C. Lee, W. Yang, and R. G. Parr, Phys. Rev. B **37**, 785 (1988).

[52] T. H. Dunning, Jr., J. Chem. Phys. **90**, 1007 (1989).